QUANTITATIVE ANALYSIS OF RADAR RETURNS FROM INSECTS

J. R. Riley
Center for Overseas Pest Research Radar Unit
Royal Signals and Radar Establishment
Great Malvern, Worcestershire, United Kingdom

INTRODUCTION

Flying insects of mass greater than a few tens of milligrams may be readily detected as individual targets by unsophisticated X-band radars and their flight trajectories conveniently shown on conventional Plan Position Indicator (PPI) displays.[1,2] Maximum detection ranges vary from a few hundred meters to several kilometers for the largest insects.

A good qualitative picture of overall insect movement may be easily obtained by direct observation of the PPI screen. However, quantitative interpretation of PPI displays in terms of aerial density, insect species and trajectory distribution is more difficult, and requires special techniques. This paper describes some of the difficulties encountered in quantitative interpretation and presents methods for dealing with them.

AERIAL DENSITY

In order to interpret the number of "dots" registered on a PPI screen in terms of aerial target density, one needs to know the volume of air sampled by the radar beam as it rotates. Unfortunately the radiation projected by an antenna does not form a sharp edged beam, but decreases gradually in intensity away from the beam axis, and also becomes weaker with increasing range. Thus small targets may be detected at short range and close to the beam axis, while larger targets are detectable at greater ranges and when further from the axis of the beam. The sampled volume thus becomes a function of target "size" or radar cross-section. This effect is illustrated in Figure 1 and a method of calculating swept volume as a function of target size is shown in Appendix I.

The radar cross-section of an insect is usually aspect sensitive[2,3,4] and so, in consequence, the swept volume becomes a function of presented aspect,[5] as well as of insect size. In normal field conditions a variety of insect types may be present at the same time, each type presenting a variety of aspects. It then becomes necessary to

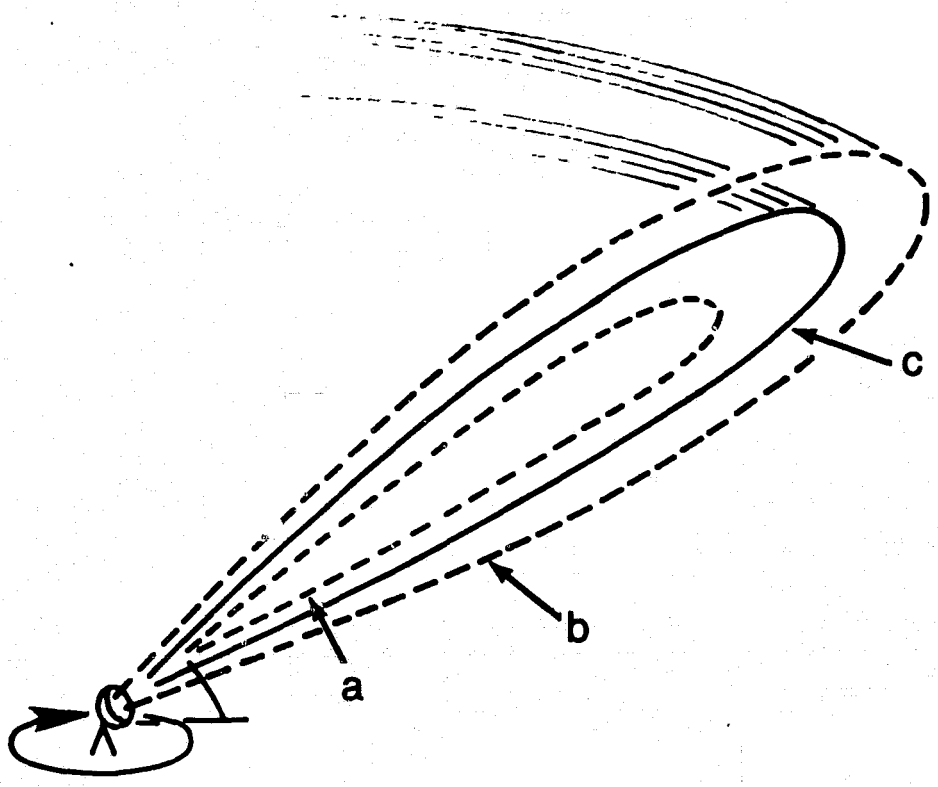

Figure 1. Scanned Volume and Detection Envelopes. The volume swept out for a particular target size is defined by the appropriate detection envelope (c). Larger (b) and smaller (a) targets merit correspondingly larger and smaller envelopes. Note that at the longer ranges, the volume swept out for smaller targets is zero.

either (a) assume a typical sampled volume, calculated for the average cross-section presented by the insect targets detectable by the radar at the range of interest, or (b) to use a procedure of the type shown in Appendix I to establish the actual target cross section distribution.

If several insects are present in the radar pulse volume (for our radars typically 10^4 m^3), interference between the targets causes large fluctuations in signal size, and the targets register irregularly on the screen. Quantitative measurements in these conditions are not usually possible. On the other hand, if the aerial density is sufficient to ensure that many (>10) targets are present in a pulse volume, volume reflectivity measurements[6] may be used to estimate density, provided that the average cross-section presented by individual targets is known. The echoes on the PPI screen in these cases are, of course, of the "solid" distributed type, and individual trajectories are not accessible.

TRAJECTORY DISTORTION AND BIAS EFFECTS

The representation on a flat surface (the PPI screen) of targets detected by a radar, which is scanning with an elevated "pencil" beam, introduces distortion into the displayed trajectories. The distortion, which is a geometrical effect, becomes significant at beam elevations above 25° and affects both direction and displacement speed of the displayed targets. One effect of this distortion is to introduce an artificial spread in the target heading distribution (see Figure II.3).

Several biases also occur which cause some target trajectories to be displayed preferentially. These biases, which are described in detail in Appendix II, have three effects. Firstly, targets on tangential flight paths are more likely to produce measureable trajectories than those on radial paths. Secondly, slowly moving (for example insects flying upwind) targets are favored compared to faster targets and, thirdly, targets flying crosswind are less likely to produce measureable trajectories than up- or down-wind oriented targets.

These biases act simultaneously and combine to make accurate determination of target heading distribution from PPI displays extremely difficult, if not impossible.

CHARACTER OF RADAR RETURNS FROM INSECTS

The signal strength returned to a radar depends on its polarization, and on the target's range, position in the radar beam, and aspect to the radar. In our non-tracking radar system the position of individual targets in the beam is usually unknown and the target aspect uncertain; we have been able to make only limited use of absolute signal levels. For example, in the case of PPI scanning, the maximum range of detection of targets was interpreted in terms of maximum presented cross-section by assuming that at least some of the targets at maximum range were intercepted by the beam axis.

A more useful parameter than this absolute level is the temporal behavior of signal level. Many flying insects produce amplitude modulation of the returned radar signal, the modulation containing components at wingbeat[2,3] and breathing frequencies.[2] Wingbeat frequency provides a useful guide to insect type - small, fast beating insects being readily distinguishable from larger, slower beating types. In many of our field studies, however, a mixture of insects of similar size have been present, and the intra-species spread and inter-species overlap of wingbeat frequency precluded positive identification.[7]

The sensitivity of a target's radar cross-section to radar polarization can also provide clues about target identity.[8,9] Unfortunately, for arbitrary target aspect,

simultaneous measurements of cross polarized return amplitude and relative phase are required and the equipment requirements are complex. We have attempted to avoid this complexity by using a supplementary radar system in which the aspect changes of targets are severely limited. This system projects a circularly symmetric beam vertically upwards in a similar manner to the systems used by Atlas *et al.*[10] and Eastwood,[11] but with the additional feature that the plane of polarization of the beam is continuously rotated (Fig. 2). Targets overflying this radar are thus exposed to controlled changes in polarization, and the consequent variation of returned signal amplitude may be interpreted in terms of body geometry. For example, semi-spherical targets show much less sensitivity to polarization changes than elongated targets.

If the beam is narrow, and provided that the radar cross section, σ, is not a sensitive function of presented aspect at near broadside incidence, then the instantaneous radar cross section will be determined by the target properties and the angle, θ, between the insect body axis and the radar E vector; i.e., $\sigma = f(\theta)$. Insects may be expected to modulate their geometry by wingbeat action and by breathing, so that $\sigma = F(\theta,\psi,\xi)$, where ψ and ξ are the instantaneous phase angles in the wingbeat and breathing cycles. A particular insect type might thus be characterized by a series of identification surfaces in the θ,ψ plane (Fig. 3), or alternatively by a single "surface" in θ,ψ,ξ space. Our measurements with this system in the field (Fig. 4) suggest that this appears to be the case, but regeneration of the recognition surfaces from radar data has proved difficult to implement. A more readily accessible feature in the data is the target heading which can be deduced (with 180° ambiguity) from the position of the maxima (after correction for beam-shape induced displacement) in the rotation cycle. An example of a "split" heading distribution detected by this technique is shown in Figure 5.

CONCLUSIONS

When the number of flying insects is low enough to permit their resolution as individual radar targets, it is possible to make quantitative estimates of their aerial density using the methods described in this paper. Accurate measurements of heading distribution are not, however, considered practicable using data from a PPI display. The use of a rotating polarization radar resolves this problem and also promises to enhance the wingbeat frequency method of identification.

It is nevertheless emphasized that a great deal of qualitative, but useful, flight information may rapidly be gained from simple scanning radars, and in many situations this is all that will be required for entomological work.

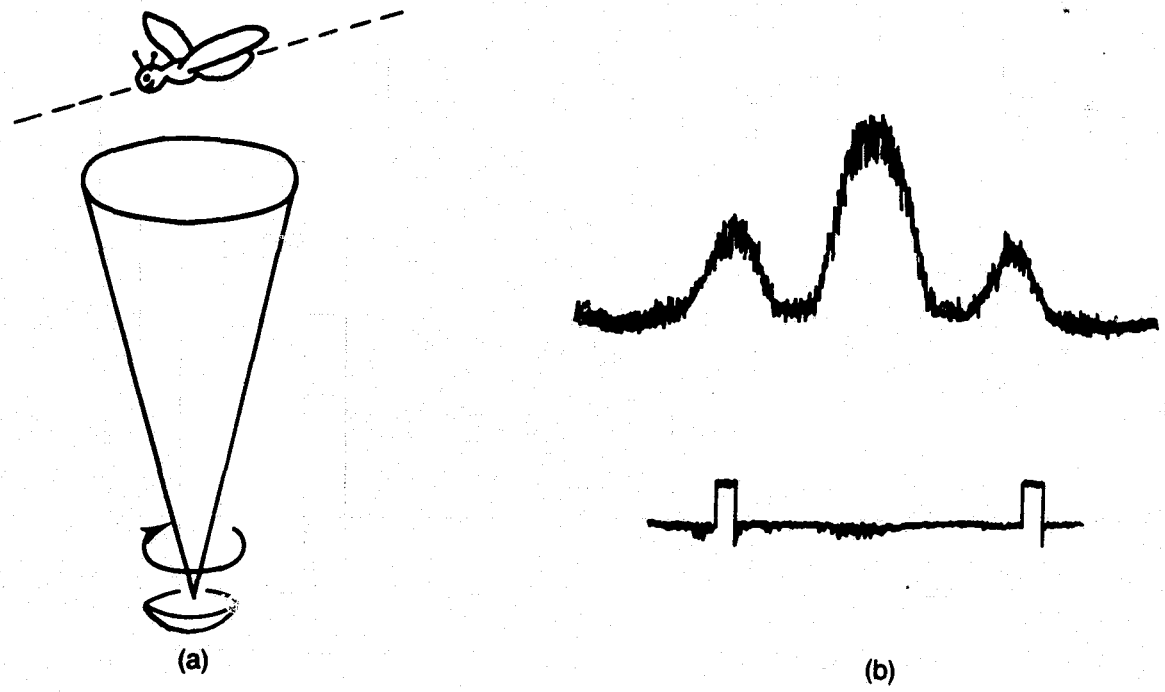

Figure 2. Vertical Looking Radar. (a) Geometry of vertical looking radar. The radar beam is stationary, but its plane of polarization is continuously rotated. (b) Typical returned signal showing wingbeat modulation superimposed on the lower frequency, large amplitude "polarization" modulation. The depth and shape of the "polarization" modulation is determined by the target body shape, long thin targets producing deeper modulation than short fat targets. Maxima normally occur when the plane of (electric) polarization is coincident with the target's longitudinal body axis. The positions of these maxima in the polarization rotation cycle thus accurately fix the target heading (with 180° ambiguity), relative to any selected reference direction. This reference direction is defined by a signal (bottom trace) generated once per feed revolution. The relative amplitude of the three largest maxima determine the beam "transit-time" and hence target displacement rate. Before "body-shape-factor," heading and displacement data can be extracted, the signals have to be corrected for the distortion produced by the (Gaussian) variation of antenna gain with target position.

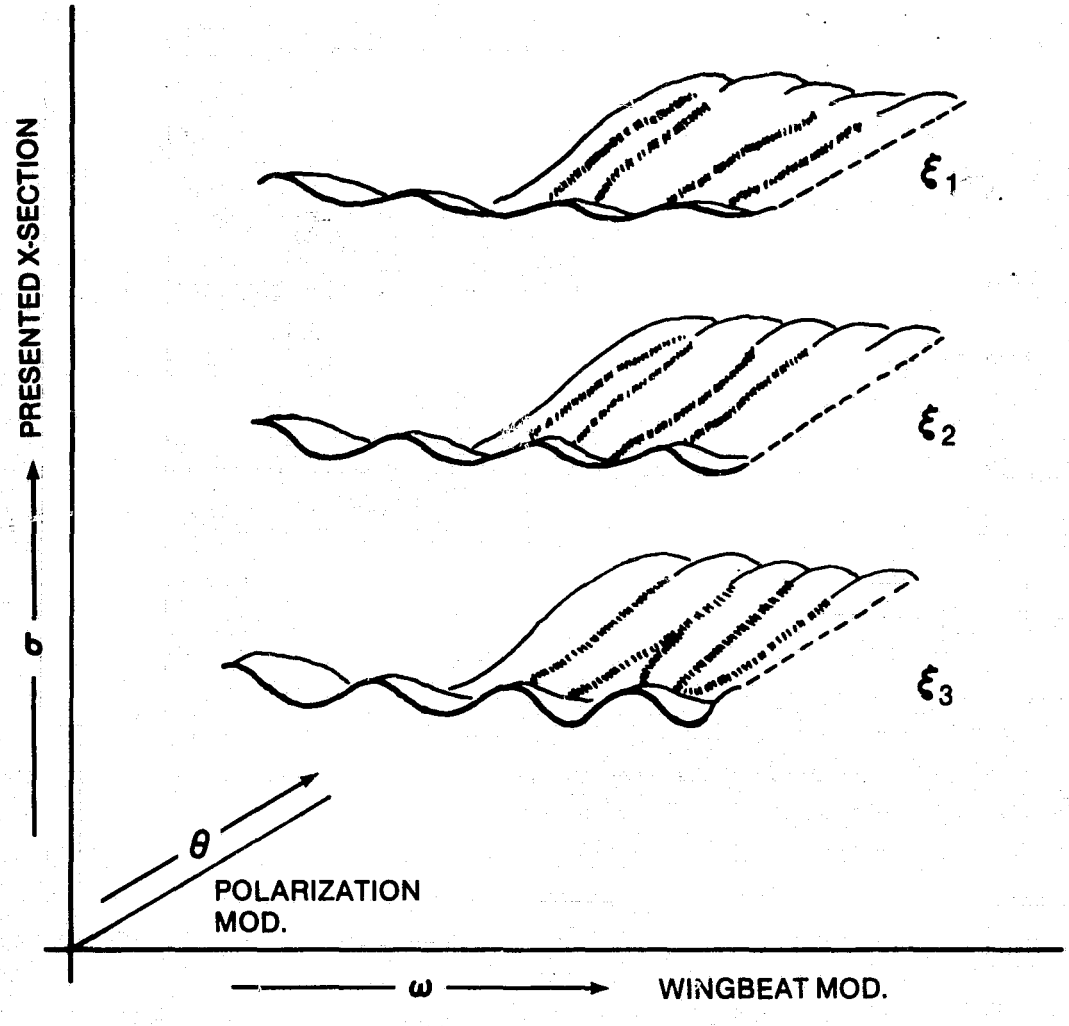

Figure 3. Possible characteristics recognition surfaces generated by exposing flying insects to a rotating polarization radar. ξ represents different breathing phase angles.

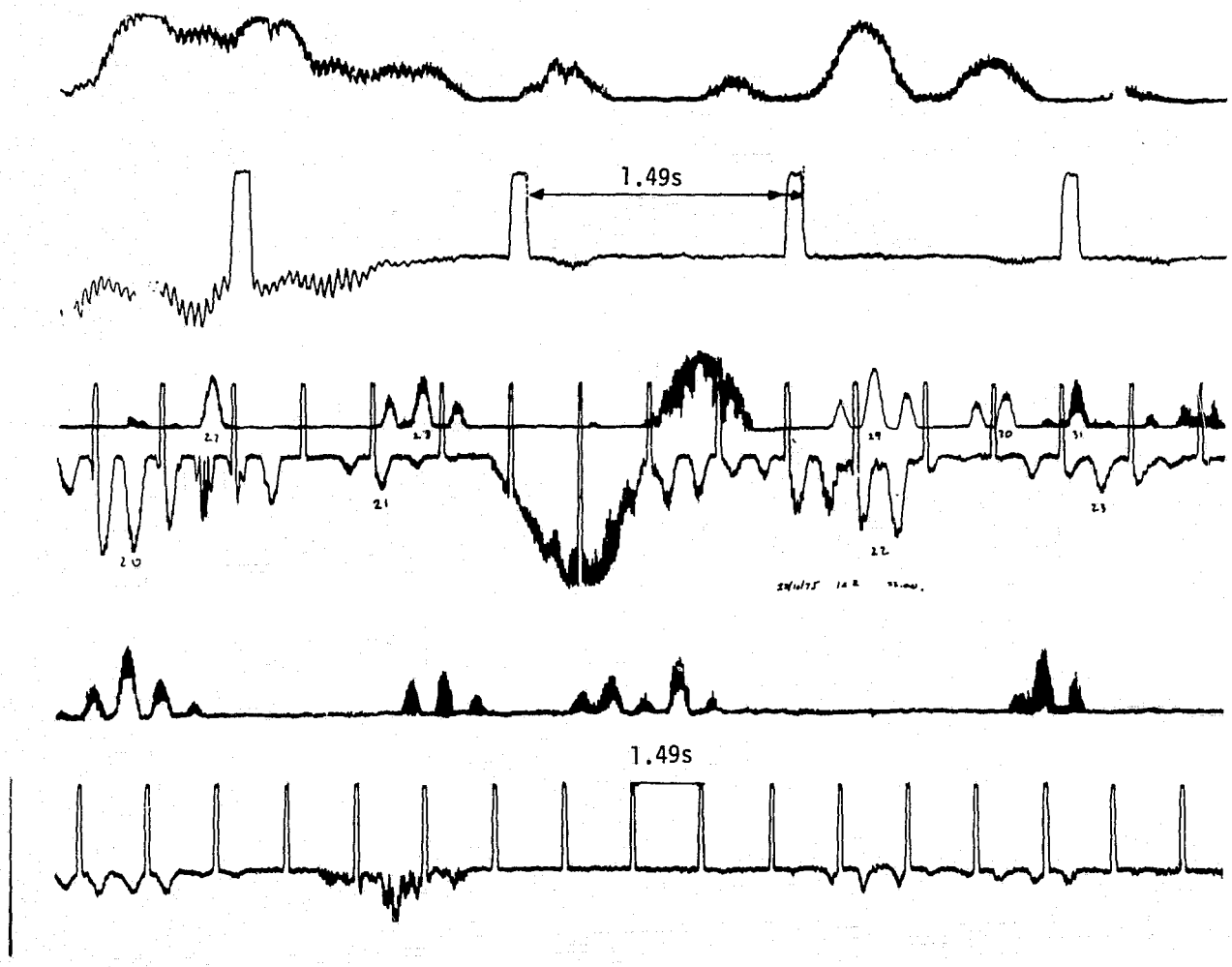

Figure 4. Examples of signals received by rotating polarization radar, shown on different time scales. The repeated rectangular pulse superimposed on one channel is the 'heading marker' signal inserted once per feed revolution.

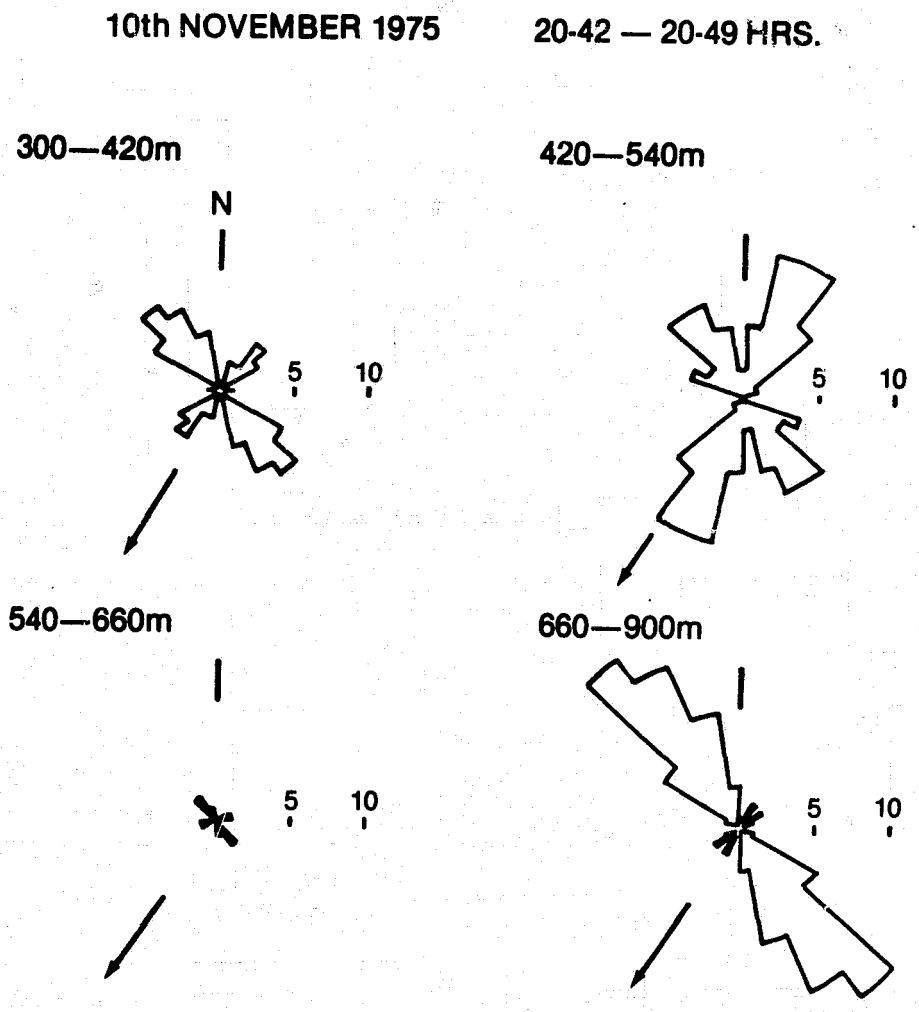

Figure 5. Distribution of insect headings at four altitudes in the range 300-900 m measured by the vertical looking radar at Kara, 20.42 - 20.49 hrs on 10th November 1975. Numbers on the radial scale show the number of targets in each 6° heading interval. The arrows show the direction of pilot balloon displacement at the same altitude and times.

REFERENCES

1. Riley, J. R., 1974: "Radar Observations of Individual Desert Locusts," Bull. Ent. Res., 64, 19-32.
2. Schaefer, G. W., 1976: "Radar Observations of Insect Flight," Symp. Roy. Ent. Soc., No. 7.
3. Riley, J. R., 1973: "Angular and Temporal Variations in the Radar Cross Sections of Insects," Proc. IEE, 120, No. 10, 1229-1232.
4. Hajovsky, R. G., Deam, A. P., and LaGrone, A. H., 1966: "Radar Reflections from Insects in the Lower Atmosphere," IEEE Trans., AP-14, No. 2, 224-227.
5. Riley, J. R., 1975: "Collective Orientation in Night Flying Insects," Nature, Vol. 253, No. 5487, 113-114.
6. Battan, L. J., 1973: "Radar Observations of the Atmosphere," Univ. Chicago Press.
7. Riley, J. R., and Reynolds, D. R., 1978: "Radar-Based Studies of the Migratory Flight of Grasshoppers in the Middle Niger Area of Mali," Proc. Roy. Soc., London (in press).
8. Copeland, J. R., 1960: "Radar Target Classification by Polarization Properties," Proc. IRE, 48, 1290-1296.
9. Tompkins, R. D., 1964: "Polarization Aspects of Radar Reflectivity Measurements," Symposium MIT Lincoln Lab., April 1964, Rept. No. RADC-TDR-64-25, Rome Air Development Center, New York.
10. Atlas, D., Harris, F. I., and Richter, J. H., 1970: "The Measurement of Point Target Speeds with Incoherent Non-Tracking Radar," 14th Radar Meteorology Conf., Tucson, Arizona, 73-78.
11. Eastwood, E., 1967: Radar Ornithology, Methuen & Co. Ltd., London, 201.
12. Skolnik, M. I., 1962: Introduction to Radar Systems, McGraw-Hill Book Co., (Int. Student Ed.).

APPENDIX I

VOLUME SAMPLED BY A RADAR AS A FUNCTION OF TARGET RADAR CROSS-SECTION

A method of calculating the volume sampled by a radar for different target sizes is outlined below, and some typical values for an X-band radar are given.

ISO-ECHOIC CONTOURS OR DETECTION LOBES

The gain of a circular parabolic antenna in an off-axis direction θ, may be described by the expression[12]

$$G_\theta = G_0 \exp\left(-2.776 \frac{\theta^2}{\theta^2_{3dB}}\right)$$

where G_0 is the on-axis gain and θ_{3dB} is the half power width of the beam. The signal power $P_{\theta,r}$ received from an off-axis, isotropically scattering, target is proportional to the square of the antenna gain, and inversely proportional to the fourth power of the target-to-radar range, r.

Thus,
$$P_{\theta,r} = \frac{C}{r^4} \exp\left(-2 \times 2.776 \frac{\theta^2}{\theta^2_{3dB}}\right)$$

where C is a constant determined by the radar properties and target radar cross section, σ_0. The locus of points (or the contour) from which this target will return signals of equal amplitude is determined by setting $P_{\theta,r}$ equal to a constant. Thus, if $P_{\theta,r} = P_{0,r_0}$, where P_{0,r_0} is the power received from the target when on-axis at range r_0, then

$$r = r_0 \exp\left(\frac{-2 \times 2.776}{4} \frac{\theta^2}{\theta^2_{3dB}}\right)$$

Figure I.1 shows an example of the contour derived from this expression for two sizes of antenna.

Targets of different sizes will return signals of the same power from different contours. Thus, for a target of size σ_n, the value of r at $\theta = 0$ is given by $r_{0,n}$, where

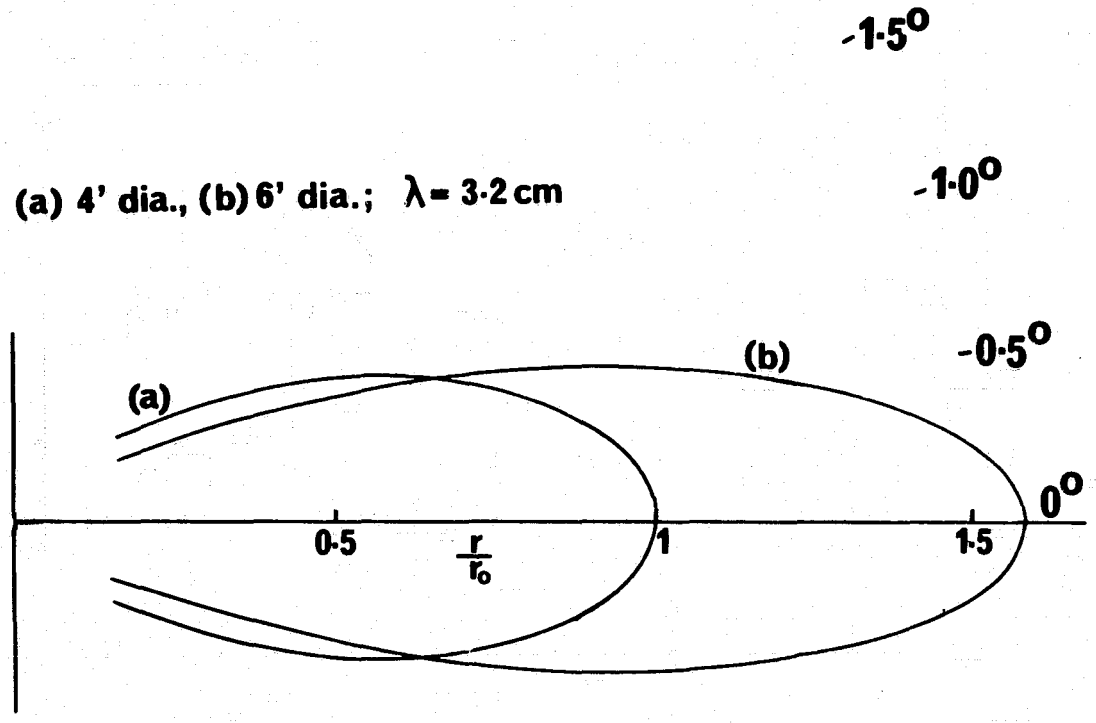

Figure I.1. Isochoic contours for two parabolic antennas. Angular scale is multiplied by 10 to make diagram clear. $\frac{r}{r_o}$ normalized to unity for on-axis signal of 4' dish.

$$\frac{r_{o,n}}{r_o} = \left(\frac{\sigma_n}{\sigma_o}\right)^{1/4}$$

so that $r_{n,\theta}$, the value of r describing the contour for target of size σ_n, is

$$r_{n,\theta} = \left(\frac{\sigma_n}{\sigma_o}\right)^{1/4} r_o \exp\left(\frac{-2.776}{2} \frac{\theta^2}{\theta^2_{3dB}}\right)$$

Figures I.2 and I.3 show, in different ways, a series of contours for different target sizes. The ratio, N, of target sizes is expressed in the diagram in decibels, thus

$$N = 10 \log \frac{\sigma_n}{\sigma_o}$$

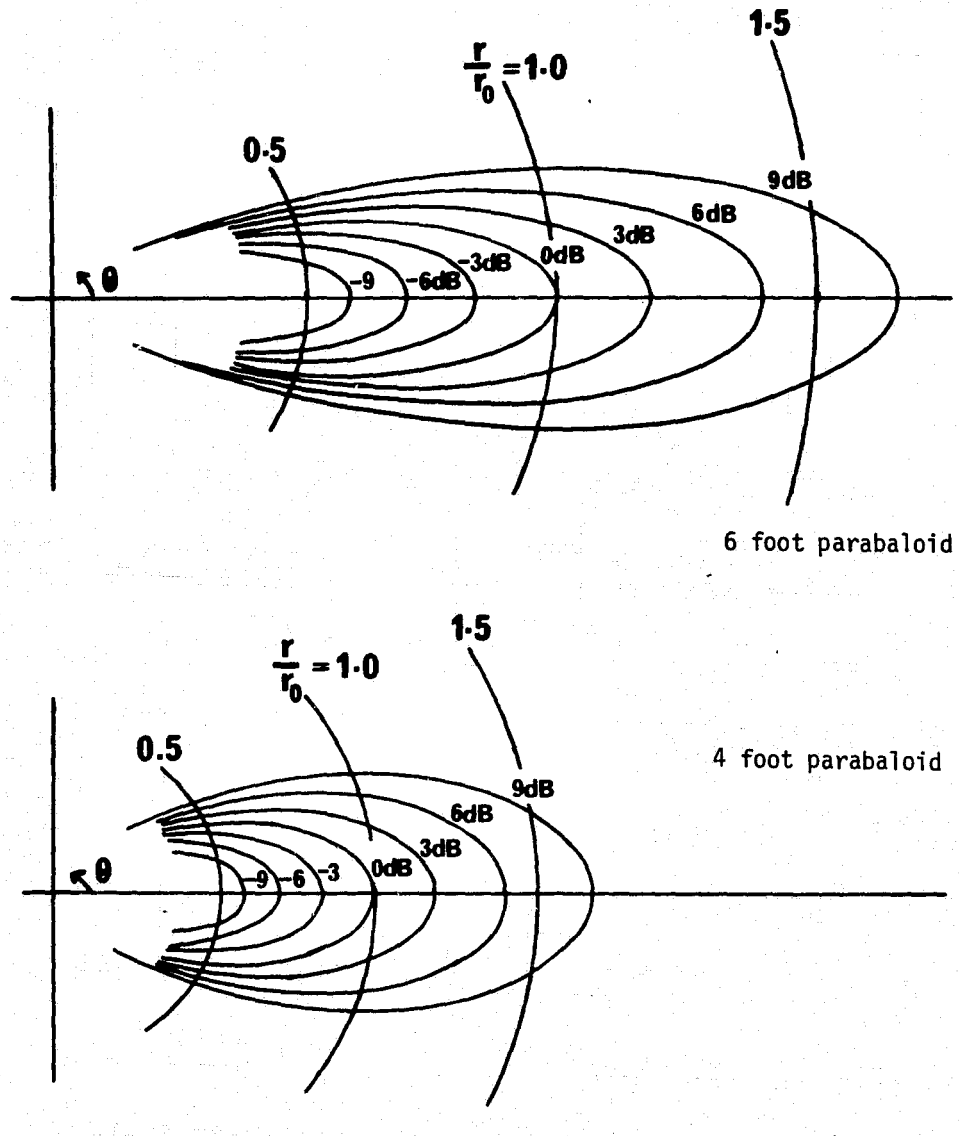

Figure I.2. Detection contours of 6' and 4' parabaloids displayed on same scale. (λ = 3.2 cm). Angular scale multiplied by 10.

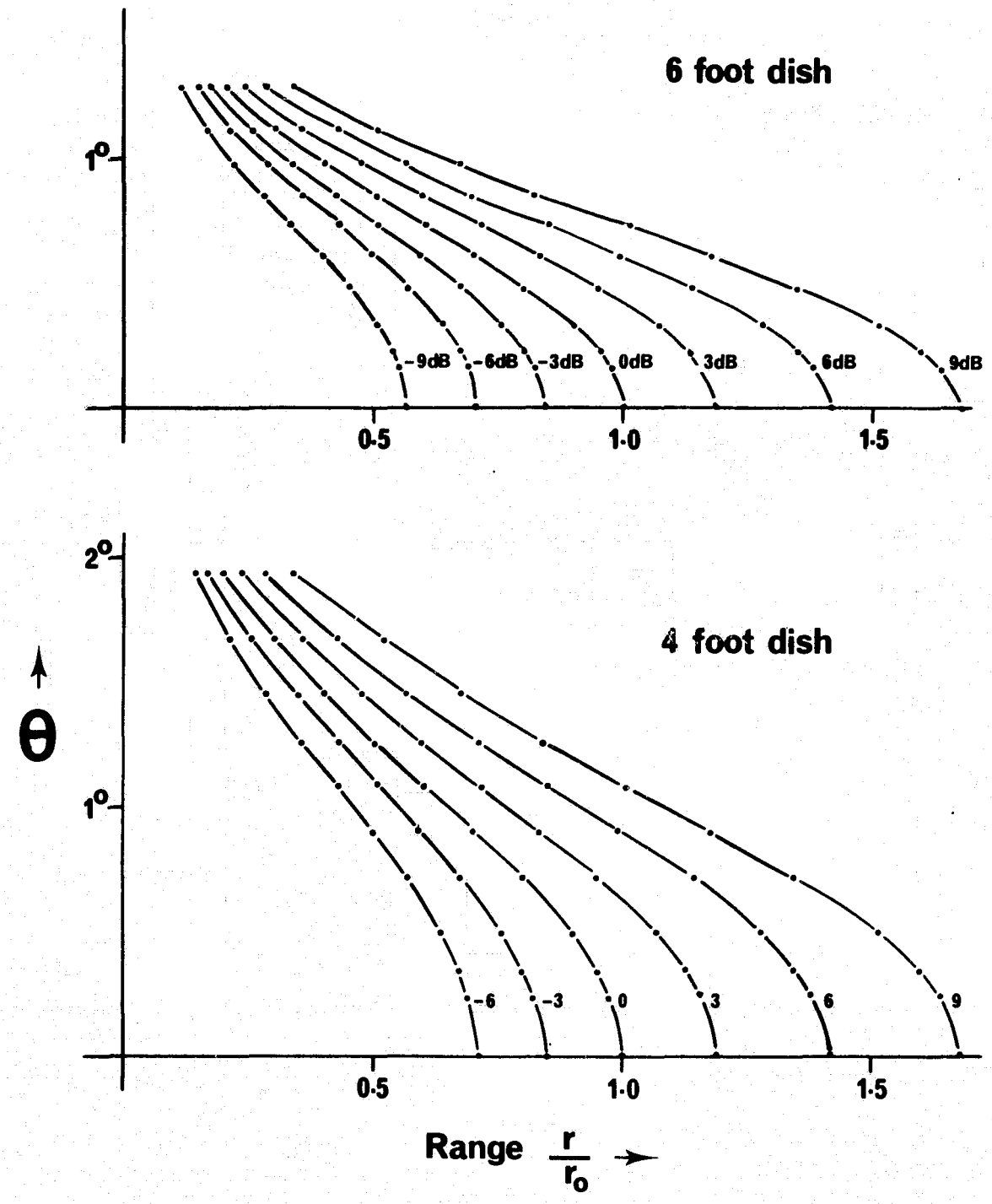

Figure I.3. Detection Envelopes.

SWEPT VOLUME

If the radar threshold is adjusted to a level corresponding to the signal received from a particular on-axis target, then targets presenting the same radar cross-section will be detected if they occur anywhere within the corresponding contour. The contour will sweep out a volume of space when the antenna is rotated (Fig. I.4) and this is the volume effectively sampled for targets of the selected cross-section.

The detection envelopes are defined by the equation

$$G_o^2 \exp\left(-2 \times 2.776 \frac{\theta^2}{\theta_{3dB}}\right) \frac{1}{r^4} = \text{constant} \qquad \text{(i)}$$

where the constant has a value appropriate for the radar performance and target size. The volume swept out is

$$V_s = \frac{4}{3} \pi \cos\varepsilon \int_0^{\theta_m} r^3 d\theta \qquad \text{(ii)}$$

where (i) defines the (r,θ) relation and θ_m is determined by the selected minimum range. Equation (ii) is then evaluated with error function integrals.

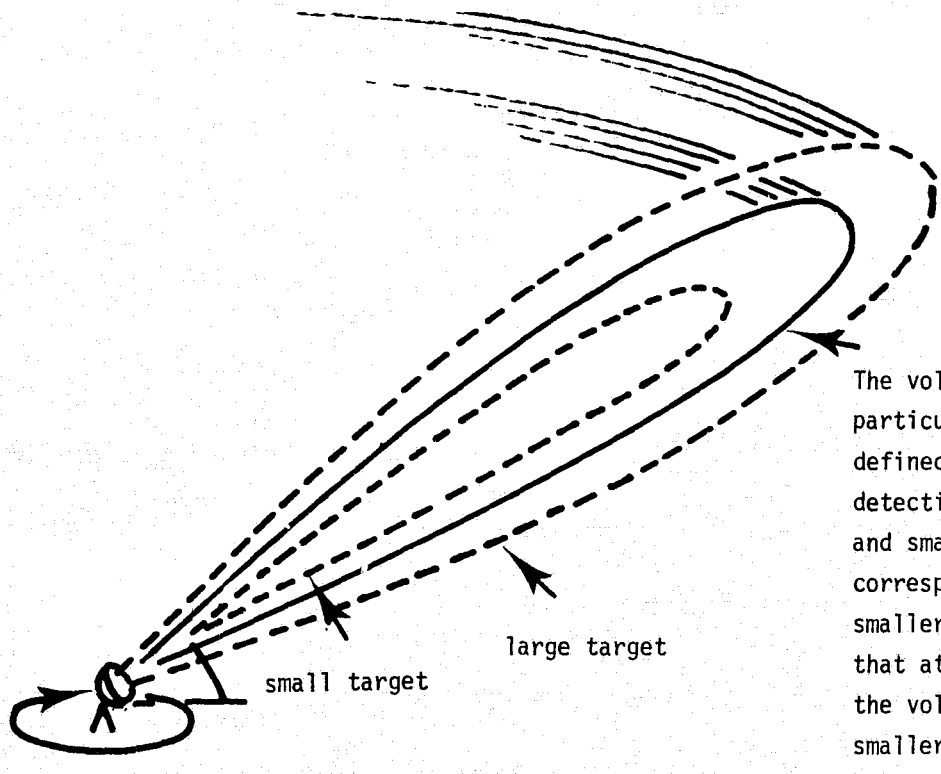

The volume swept out for a particular target size is defined by the appropriate detection envelope. Larger and smaller targets merit correspondingly larger and smaller envelopes. Note that at the longer ranges, the volume swept out for smaller targets is zero.

Figure I.4. Scanned Volume and Detection Envelopes.

One method of establishing aerial densities is to make a "dot" count in the annulus between two selected ranges r_1 and r_2, and then to calculate the volume swept out between these two ranges by the appropriate contour. Using Figure I.5 as a reference this volume is calculated as follows:

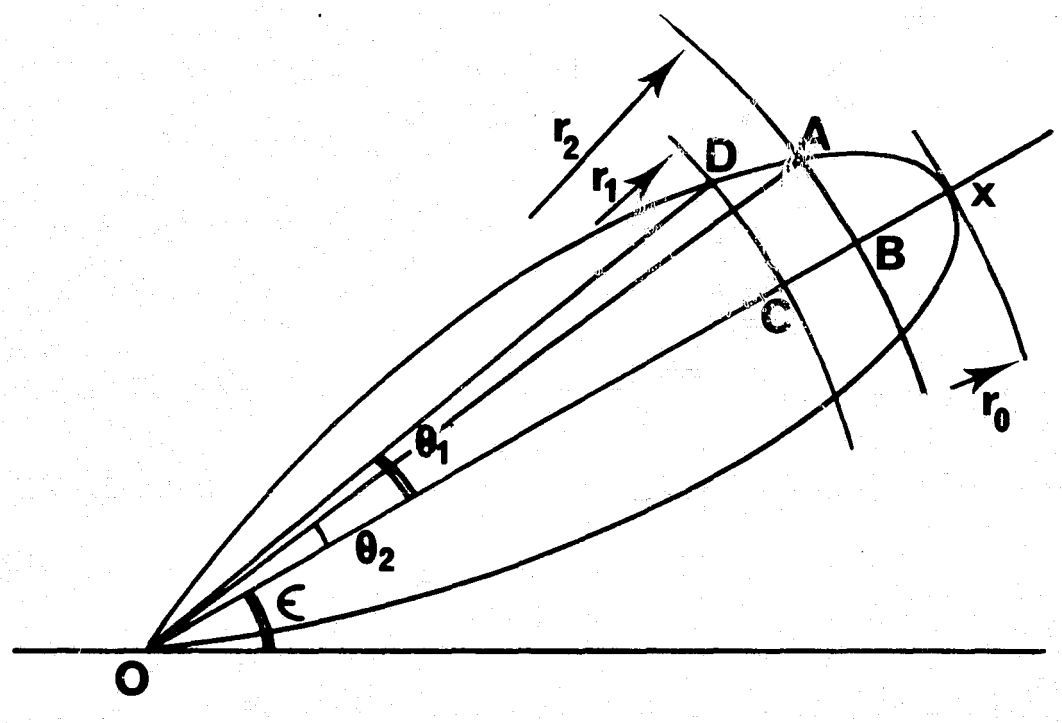

Figure I.5. Volume swept out between two ranges.

The volume swept out by annulus between r_1 and r_2 is

$$V_s = 2 \times (\text{Vol. swept out by DXC} - \text{Vol. swept out by AXB}) \qquad \text{(iii)}$$

$$\left.\begin{aligned} \text{But Vol DXC} &= \text{Vol ODXCO} - \text{Vol ODC}, \\ \text{and Vol AXB} &= \text{Vol OAXBO} - \text{Vol OAB} \end{aligned}\right\} \qquad \text{(iv)}$$

$$\text{Now, Vol OAB} = \frac{2}{3}\pi r_2^3\,\theta_2 \cos\varepsilon,\ \text{Vol ODC} = \frac{2}{3}\pi r_1^3\,\theta_1 \cos\varepsilon, \qquad \text{(v)}$$

and, using the approximation that $\cos(\varepsilon + \theta) \simeq \cos$ for small θ,

$$\text{Vol ODXCO} = \frac{1}{2} r^2 \frac{2\pi r}{3} \cos\varepsilon\, d\theta = \frac{2}{3}\pi \cos\varepsilon \int_0^{\theta_1} r^3\, d\theta \qquad \text{(vi)}$$

But for an iso-echoic contour; $r^3 = r_o^3 \exp\left(-2 \times 2.776 \times \frac{3}{4} \frac{\theta^2}{\theta_{3dB}^2}\right)$.·.

Thus, Vol ODXCO $= \frac{2}{3}\pi r_o^3 \cos\varepsilon \int_0^{\theta_1} \exp\left(\frac{-2.776 \times 3}{2} \frac{\theta^2}{\theta_{3dB}^2}\right) d\theta$.

Or, writing $\theta' = c\theta$, where $c^2 = \frac{2.776 \times 3}{\theta_{3dB}^2}$,

$$\text{Vol ODXCO} = \frac{2\pi}{3} \frac{r_o^3 \cos\varepsilon}{c} \int_0^{c\theta_1} \exp\left(\frac{-\theta'^2}{2}\right) d\theta' . \qquad \text{(vii)}$$

The same expression applies to OAXBO, except that $c\theta_2$ is the limit of integration. The integral on the RHS of equation (vii) is the error function integral which may be evaluated from standard tables. So we may write

$$\text{Vol ODXCO} = \frac{2\pi}{3} r_o^3 \frac{\cos\varepsilon}{c} \times I_2.$$

But $r_o = r_2 \times 10^{\frac{N}{40}}$, where N is the number of dB's by which the level of the iso-echoic contour being used exceeds that of the contour passing through point B.

Thus, $$\text{ODXCO} = \frac{2\pi}{3} r_2^3 \frac{\cos\varepsilon}{c} 10^{\frac{3N}{40}} I_2 . \qquad \text{(viii)}$$

Hence from (iii), (iv), (v), and (viii)

$$V_s = \left[\frac{10^{\frac{3N}{40}}}{c} (I_1 - I_2) + (\theta_2 - \alpha^3\theta_1)\right] \frac{4}{3}\pi r_2^3 \cos\varepsilon$$

where $\alpha = \frac{r_1}{r_2}$; θ_1 and θ_2 are read from Fig. I.3 at $\frac{r}{r_o} = \alpha$ and 1; and I_1 and I_2 are obtained from error function tables.

But the volume swept out by a cone of semi-angle equal to the antenna "3dB" angle is

$$V_{3dB} = \frac{2}{3}\pi r_2^3 \theta_{3dB} (1 - \alpha^3) \cos\varepsilon$$

Thus,

$$\beta = \frac{V_s}{V_{3dB}} = \frac{\left[\frac{10^{\frac{3N}{40}}}{c} (I_1 - I_2) + (\theta_2 - \alpha^3\theta_1)\right] \times 2}{\theta_{3dB} (1 - \alpha^3)}$$

Figure I.6 shows the results of evaluating this equation, and allows one to read off the swept volume in terms of target size relative to a known target. An example of this is shown below.

1. From calibration flight experiments, note r_c the maximum range for PPI detection of the calibration target of known size, σ_c, (at the usual gain and attenuation settings).

2. Then use these two figures to calculate the minimum target size (σ_m) detectable on axis at r_2, the outer band of the measuring annulus. Thus

$$\sigma_m = \sigma_c \left(\frac{r_2}{r_c}\right)^4$$

3. Next calculate the ratio of σ_m to the expected target cross-section σ_t

$$N = 10 \log \left(\frac{\sigma_t}{\sigma_m}\right) \text{ dB}$$

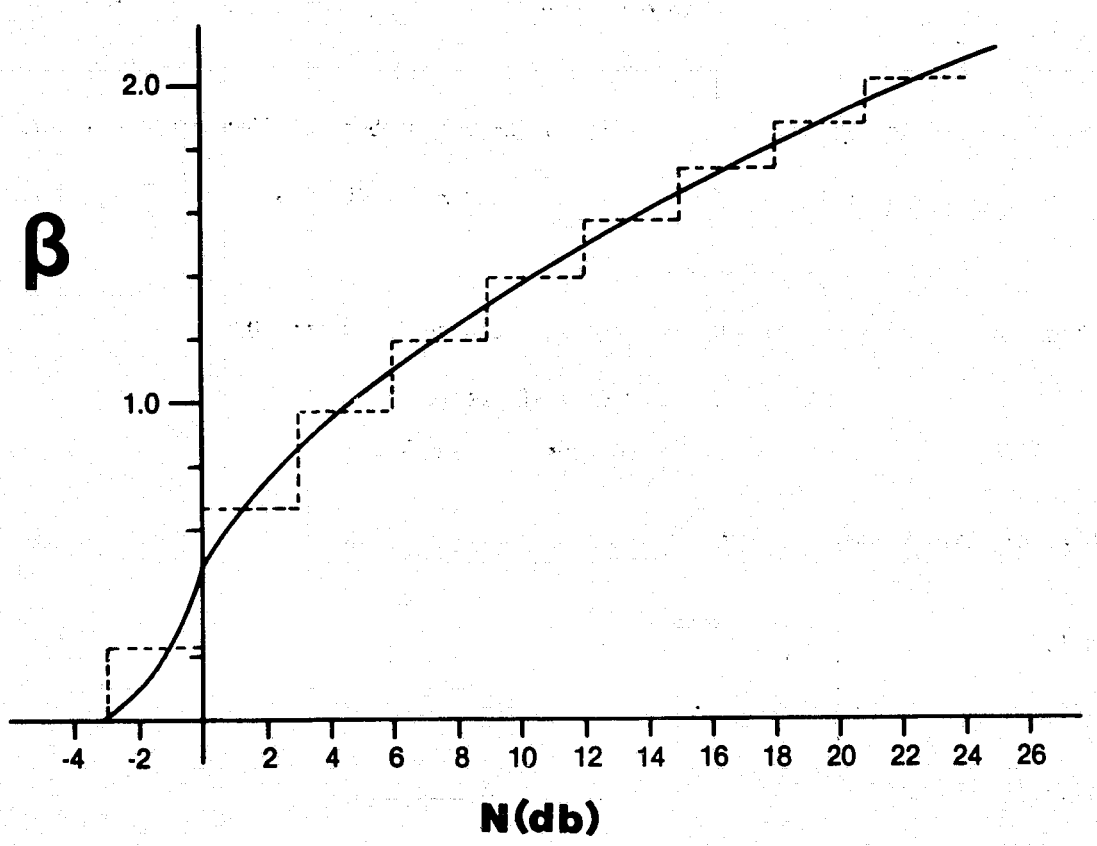

Figure I.6. Ratio of sweeping volume between r_2 and αr_2 to 3db volume as a function of target size, for a parabolic antenna, with r_2 = 1200 yd, and r_1 = 1000 yd, i.e., α = 0.83.

4. Use N, together with a graph relating N to the ratio β of swept volume to 3dB volume for the antenna (Fig. I.6) to obtain β.

5. From β and the value of the 3dB volume, calculate the swept volume;

$$\text{Volume} = V_{3dB} \times \beta$$

Example (1) (Type A Radar) $\lambda = 3.2\ cm^2$

(i) For Cu plated ping-pong ball calibration target, d = 3.78 cm and $\sigma_c = 16\ cm^2$, and $r_c = 2930$ m, $r_2 = 1096$ m (1200 yd), $r_1 = 914$ m (1000 yd) and expected target size is $0.5\ cm^2$.

(ii) $\sigma_m = 16 \left\{\frac{1096}{2930}\right\}^4 = 0.31\ cm^2$

(iii) $N = 10 \log \left\{\frac{0.50}{0.31}\right\} = 2.1\ dB$

(iv) From Fig. I.6 for a paraboloid, when $\frac{r_1}{r_2} = \frac{1000}{2000} = 0.83$; obtain, for N = 2.1 dB, $\beta = 0.68$

(v) For a 6' paraboloid, $\theta_{3dB} = 1.2°$ so 3dB volume between 1096 m and 914 m is

$$V_{3dB} = \frac{2}{3}\pi^2 \times \frac{1.2}{180} (1096^3 - 914^3) \cos\varepsilon = 2.4 \times 10^7 \cos\varepsilon \quad [m^3]$$

(expressing θ_{3dB} in radians).

Thus, the volume swept for $0.5\ cm^2$ targets between 914 m and 1096 m is

$$V_s = 2.4 \times 0.68 \times 10^7 \cos\varepsilon \quad [m^3]$$
$$= 1.6 \times 10^7 \cos\varepsilon \quad [m^3]$$

Example (2) (Type B Radar) $\lambda = 3.2\ cm^2$

(i) $r_c = 5030$ m

(ii) $\sigma_m = 16 \left\{\frac{1096}{5030}\right\}^4 = 3.6 \times 10^{-2}\ cm^2$

(iii) $N = 10 \log \left\{\frac{0.50}{3.6 \times 10^{-2}}\right\} = 11.4\ dB$

(iv) From graph; for N = 11.4 dB, $\beta = 1.42$

Thus, (v) $V_s = 2.4 \times 10^7 \times 1.42$

$= 3.4 \times 10^7 \cos\varepsilon \quad [m^3]$

It should be pointed out that the registration of a target above a selected threshold is a statistical process, and depends on the temporal behavior of the target cross-section, as well as the required false alarm and detection probabilities.[12] The contours shown in Figure I.1 thus represent diffuse boundaries between the size categories, rather than precise limits.

MEASUREMENT OF TARGET SIZE DISTRIBUTION

Normally a range of different target cross-sections may be present, and it is necessary to establish the distribution of these cross-sections in order to produce accurate measurements of target density. The problem may be illustrated by pointing out that the volume calculated above for targets presenting cross-sections of 0.5 cm^2 is also sensitive in different proportions to larger and smaller targets.

A method of measuring size distribution is shown below.

Objective

To determine the number of aerial targets per unit volume in each 3dB size interval, starting at 10 cm^2 down to 0.1 cm^2.

(i) From calibration flight results note r_c, the maximum range for a target of size σ_c (typically 16 cm^2).

(ii) Calculate the minimum cross-section σ_m detectable at r_2, the outer edge of the measuring annulus.

$$\sigma_m = \sigma_c \left\{\frac{r_2}{r_c}\right\}^4$$

(iii) Calculate the ratio N, where

$$N = 10 \log \left\{\frac{10}{\sigma_m}\right\} \text{ dB}$$

To obtain the amount (N) by which the radar threshold must be increased so that targets presenting cross-sections of 10 cm^2 will just be detected on axis at r_2.

(iv) Increase the radar threshold by this amount. The radar is now scanning an average volume $\simeq V_{3dB} \times 0.2$ for targets in the range 10 - 5 cm^2 (See Fig. I.6).

(v) Decrease the IF attenuation by 3dB. The radar is now scanning a volume of 0.68 x V_{3dB} for 10-5 cm^2 targets, plus a volume of 0.2 x V_{3dB} for 5-2.5 cm^2 targets.

(vi) Decrease the IF attenuation by a further 3dB. The radar is now scanning a volume of 0.98 x V_{3dB} for 10 - 5 cm^2 targets, 0.68 x V_{3dB} for 5 - 2.5 cm^2 targets plus 0.2 x V_{3dB} for 2.5 - 1.25 cm^2 targets.

Repeat until 21 dB of IF attenuation has been removed (or normal operating level is reached). Then, if N_1 is the number of targets registered with the first setting,

$$N_1 = n_1 \times 0.2 \times V_{3dB}$$

where n_1 is the aerial density of targets in the range 10-5 cm^2.

If N_2 is the number of targets registered after the decrease of IF attenuation by 3dB

$$\frac{N_2}{V_{3dB}} = n_1 \times 0.68 + n_2 \times 0.2$$

where n_2 is the aerial density of targets in the range 5 - 2.5 cm^2.

Similarly,

$$\frac{N_3}{V_{3dB}} = n_1 \times 0.98 + n_2 \times 0.68 + n_3 \times 0.2$$

$$\frac{N_4}{V_{3dB}} = n_1 \times 1.20 + n_2 \times 0.98 + n_3 \times 0.68 + n_4 \times 0.2$$

$$\frac{N_5}{V_{3dB}} = n_1 \times 1.40 + n_2 \times 1.20 + n_3 \times 0.98 + n_4 \times 0.68 + n_5 \times 0.2$$

$$\frac{N_6}{V_{3dB}} = n_1 \times 1.58 + n_2 \times 1.40 + n_3 \times 1.20 + n_4 \times 0.98 + n_5 \times 0.68 + n_6 \times 0.2$$

$$\frac{N_7}{V_{3dB}} = n_1 \times 1.75 + n_2 \times 1.58 + n_3 \times 1.40 + n_4 \times 1.20 + n_5 \times 0.98 + n_6 \times 0.68 + n_7 \times 0.2$$

The aerial densities of the different groups (n_n) may then be extracted from these equations by sequential solution.

An alternative method is to determine the amplitude distribution of the signals received by the radar whilst scanning, and to use a similar procedure to that outlined above. This method requires, however, a knowledge of the radar IF amplifier and video detector responses.

APPENDIX II

DISTORTION AND BIAS EFFECTS IN PPI SCANNING

The trajectories of targets which subtend finite angles of elevation from a radar become distorted when displayed on a PPI screen. The distortion, which affects both velocity and target direction, becomes serious above elevation angles of 30°.

On the PPI (see Fig. II.1) the apparent velocity, V_a, is

$$V_a^2 = \left(\frac{dr}{dt}\right)^2 + \left(\frac{r d\theta}{dt}\right)^2 . \qquad \text{(i)}$$

But for horizontal straight flight the true velocity, V_t, is

$$V_t = \frac{d}{dt} \quad (a \tan \theta)$$

$$= a \sec^2 \theta \frac{d\theta}{dt}$$

$$= r \cos \varepsilon \sec \theta \frac{d\theta}{dt}$$

so

$$\frac{d\theta}{dt} = \frac{V_t \cos \theta \sec \varepsilon}{r} \qquad \text{(ii)}$$

And from geometry $r^2 = h^2 + a^2 \sec^2 \theta$; so,

$$\frac{dr}{dt} = r \tan \theta \cos^2 \varepsilon \frac{d\theta}{dt} \qquad \text{(iii)}$$

Thus, from (ii) and (iii)

$$\frac{dr}{dt} = V_t \cos \varepsilon \sin \theta \qquad \text{(iv)}$$

(iv) and (ii) in (i) give

$$\frac{V_a}{V_t} = \left\{\cos^2\varepsilon \sin^2\theta + \cos^2\theta \sec^2\varepsilon\right\}^{1/2}$$

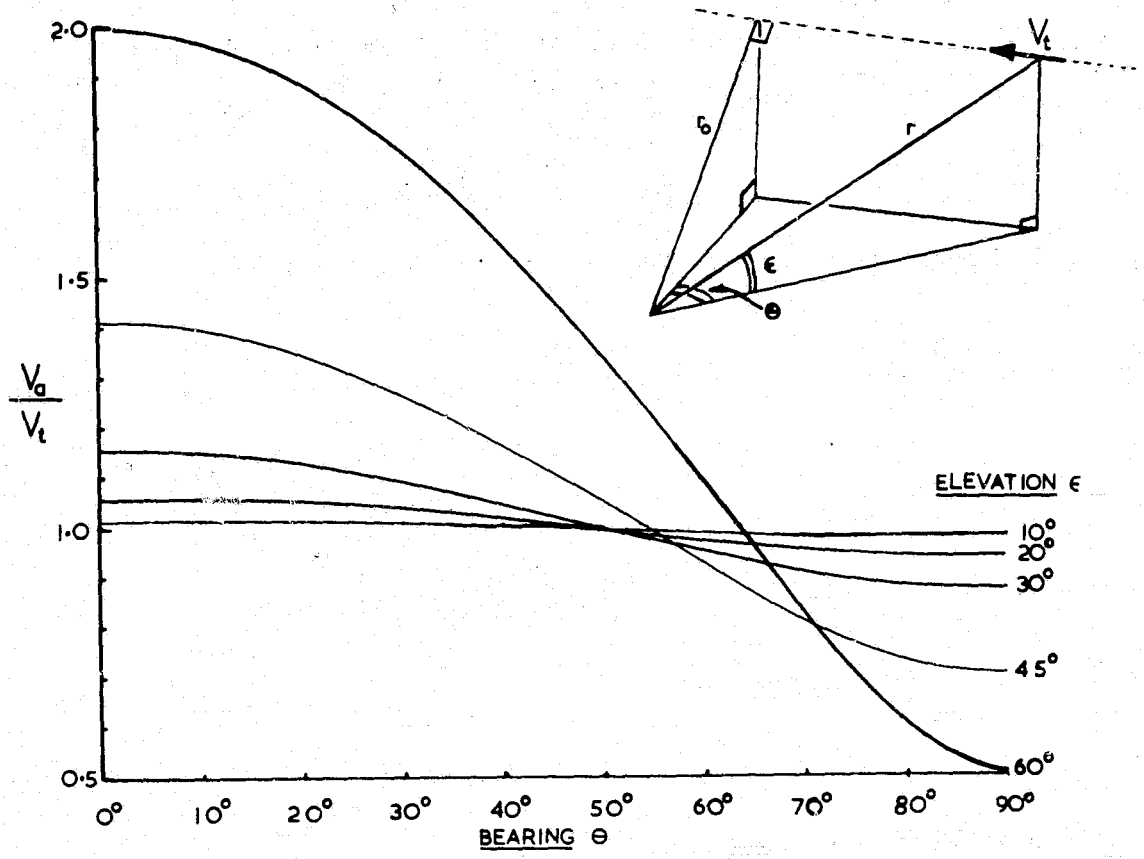

Figure II.1. The apparent velocity V_a on a PPI display of a target moving in a horizontal straight line with velocity, V_t, varies with target position and elevation. The graph illustrates this variation for a selected series of elevations. The bearing angle, θ, is measured between projections onto a horizontal plane of the target position vector, r, and r_o, the vector defining the distance of closest approach.

The apparent direction of the trajectory as displayed on the PPI is

$$\alpha = \tan^{-1}\left\{ \frac{rd\theta}{dt} \Big/ \frac{dr}{dt} \right\}$$

$$= \tan^{-1}\left\{ \frac{V_t \cos\theta \sec\varepsilon}{\tan\theta \cos^2\varepsilon \, V_t \cos\theta \sec\varepsilon} \right\}$$

$$= \tan^{-1} \left(\cot\theta \sec^2\varepsilon\right)$$

And the variation, Δ, from the true direction is

$$\Delta = \alpha + \theta - 90^\circ$$

Values of Δ and V_a/V_t are shown in Figures II.1 and II.2. The overall effect of both distortions is to increase the spread in heading distributions. Fig. II.3 gives examples of the displayed trajectories which would be produced by a group of targets all flying in exactly parallel lines.

As well as this distortion, PPI trajectories are subject to several biases, some target trajectories being displayed preferentially. The first bias varies with the azimuthal position occupied by the target when it is intercepted by the radar beam. The effect is most conveniently demonstrated by calculating the signal variation expected from isotropically scattering targets passing through the scanned volume from different positions.

Referring to Figure II.4, consider the signal returned by a target as it passes from +x through the position r_o, θ_o, ε_o to -x. At r_o, θ_o, ε_o the target is intercepted by the axis of the illuminating beam as it sweeps in azimuth, but at other positions along the +x to -x axis, the target is either above or below the beam axis, and the returned signal is consequently weaker. The maximum returned signal strength can be computed by calculating the angle subtended between the radar-target line and the beam axis at their distance of closest approach, and then using the Gaussian relation between antenna gain and distance off-axis.

For example, the r, θ, ε coordinates of the target shown in Figure II.4 may be derived thus

$$r_o \sin\varepsilon_o = r_x \sin\varepsilon_x \qquad \text{(constant altitude condition)} \qquad \text{(v)}$$

$$r_o \cos\varepsilon_o \sin\theta_o - r_x \cos\varepsilon_x \sin\theta_x = x \qquad \text{(vi)}$$

$$r_o \cos\varepsilon_o \cos\theta_o = r_x \cos\theta_x \cos\varepsilon_x \qquad \text{(vii)}$$

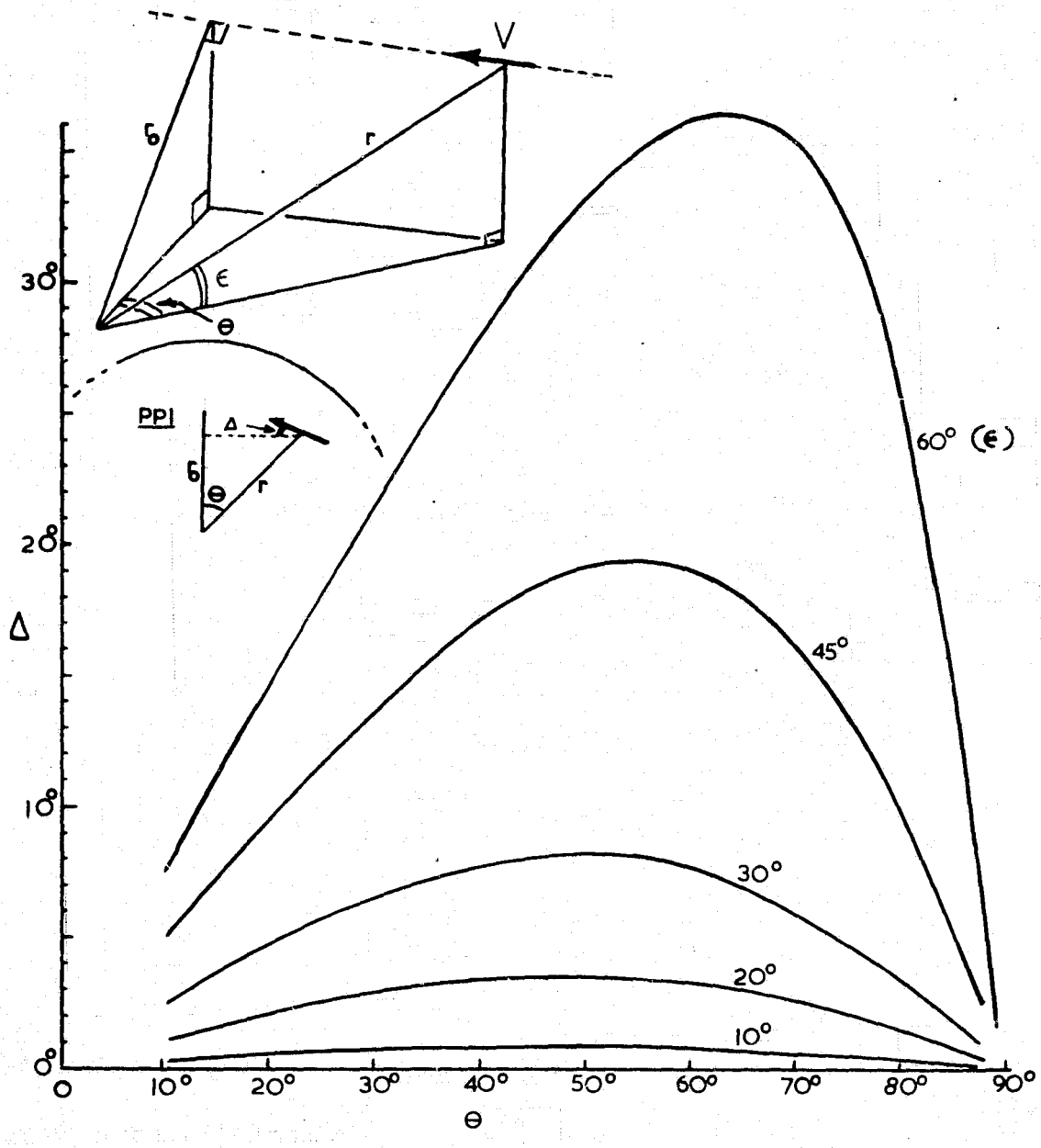

Figure II.2. The apparent direction of movement on a PPI display of a target moving in a horizontal straight line, varies with target position and elevation (ε). This graph shows the angular deviation (Δ) of the apparent direction, from the true direction, for a selected series of elevations. The 'true direction' is at right angles to r_0, the vector defining the distance of closest approach. The bearing angle θ, is measured between projections onto a horizontal plane of the target position vector r, and r_0.

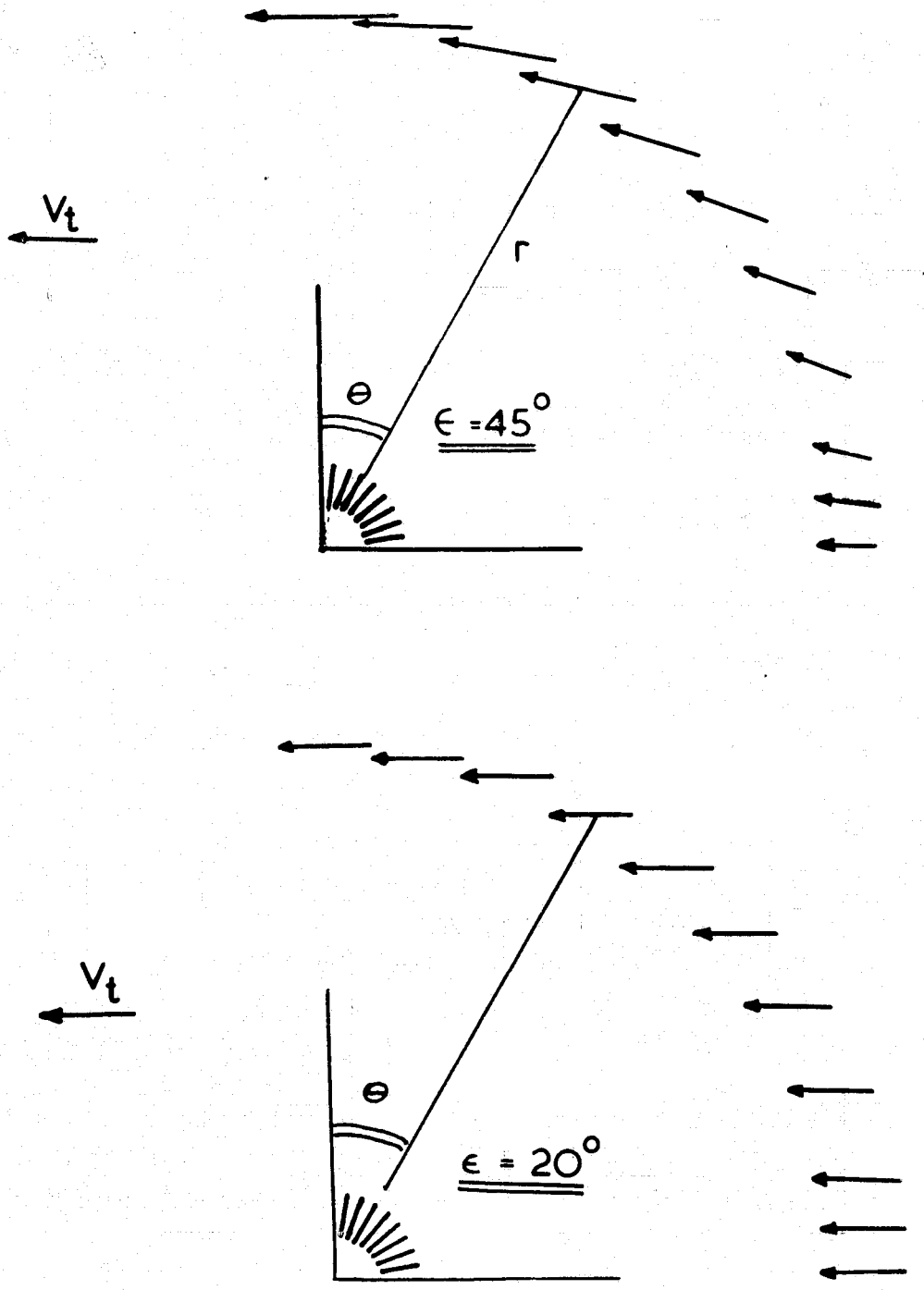

Figure II.3. Examples of the distortion of straight line horizontal trajectories displayed on a PPI system operating at finite angles of elevation (ε). The velocity vectors indicate the displayed velocity at various bearing angles (θ). The true velocity is indicated by V_t.

from (vi) and (vii),

$$\tan \theta_x = \left\{ \frac{\sin \theta_o}{\cos \theta_o} - \frac{x}{\cos \varepsilon_o} \cdot \frac{1}{\cos \theta_o} \cdot \frac{1}{r_o} \right\}$$

$$\theta_x = \tan^{-1} \left(\tan \theta_o - \frac{x}{r_o} \cdot \frac{1}{\cos \varepsilon_o \cos \theta_o} \right) \qquad \text{(viii)}$$

from (v) and (vii),

$$\frac{r_x}{r_o} = \frac{\cos \varepsilon_o \cos \theta_o}{\cos \varepsilon_x \cos \theta_x} = \frac{\sin \varepsilon_o}{\sin \varepsilon_x}$$

$$\text{so} \qquad \varepsilon_x = \tan^{-1} \left(\tan \varepsilon_o \cdot \frac{\cos \theta_x}{\cos \theta_o} \right) \text{with } \theta_x \text{ from (viii)} \qquad \text{(ix)}$$

except for $\theta_o = 90°$, when

$$\varepsilon_x = \tan^{-1} \left(\frac{r_o \sin \varepsilon_o}{r_o \cos \varepsilon_o - x} \right)$$

Thus the maximum signal returned when the beam intercepts the target is

$$S_x = S_o \left(\frac{r_o}{r_x} \right)^4 \cdot \exp \left(- 2.776 \frac{\theta^2}{\theta^2_{3dB}} \right) \qquad \text{(x)}$$

where S_o is the signal returned at range r_o. Using (v) this becomes

$$S_x = \left(\frac{\sin \varepsilon_x}{\sin \varepsilon_o} \right)^4 \cdot \exp \left[- 2.776 \left[\frac{\varepsilon_x - \varepsilon_o}{\theta_{3dB}} \right]^2 \right] \text{with } \varepsilon_x \text{ from ix.}$$

S_x is plotted in Figure II.4 as a function of x, for a variety of values of θ_o (azimuthal position), and it can be seen that the distance along the +x to -x trajectory for which the signal is above a threshold (say $S/S_o = 0.3$) is much greater for $0 < \theta° < 25°$ (i.e. tangential targets) than in other quadrants. Thus the chances of producing enough "hits" on a passing target to produce a measurable trajectory are greater if the target passes along a tangential rather than radial path. The bias is not a serious problem if targets are equally distributed around the radar, because no particular direction of flight is favored.

A more serious bias is generated by target displacement speed. During the time that a target moves along an axis -x to +x, the radar beam rotates several times, producing several hits. If the translation velocity along x is high, the time available for beam rotations is reduced, so the number of hits, and therefore the chances of producing a measurable trajectory are also reduced. It is clear that measurements, for example, of

the proportion of down-wind orientated (and therefore faster) targets are therefore biased in favor of the slower, up-wind targets. Allowance can be made for this bias by measuring trajectory velocities, and correcting the distribution accordingly.

The most serious bias of all is caused by the fact that most insect targets do not scatter isotropically. Thus in equation (x) one has to include a term which recognizes the aspect dependence of the target cross section, $\sigma(\phi)$. We write

$$S_o = \left(\frac{\sin \varepsilon_x}{\sin \varepsilon_o}\right)^4 \cdot \exp\left[-2.776\left(\frac{\varepsilon_x - \varepsilon_o}{\theta_{3dB}}\right)^2\right] \sigma(\phi)$$

The angular variation of cross-section of *Locusta* may, for example, be approximately described by the relation

$$\sigma(\phi) = 2.4\left[2.7\left(\exp\left(-\frac{2.78}{14}\phi^2\right)\right) + 0.2\right] \quad [cm^2]$$

This equation has been used with equation (x) to compute the curves shown in Figure II.5, which illustrate the complex relation between signal strength, heading and angular position. Unless the target's angular variation of cross-section is known, quantitative correction for this biasing effect is not possible.

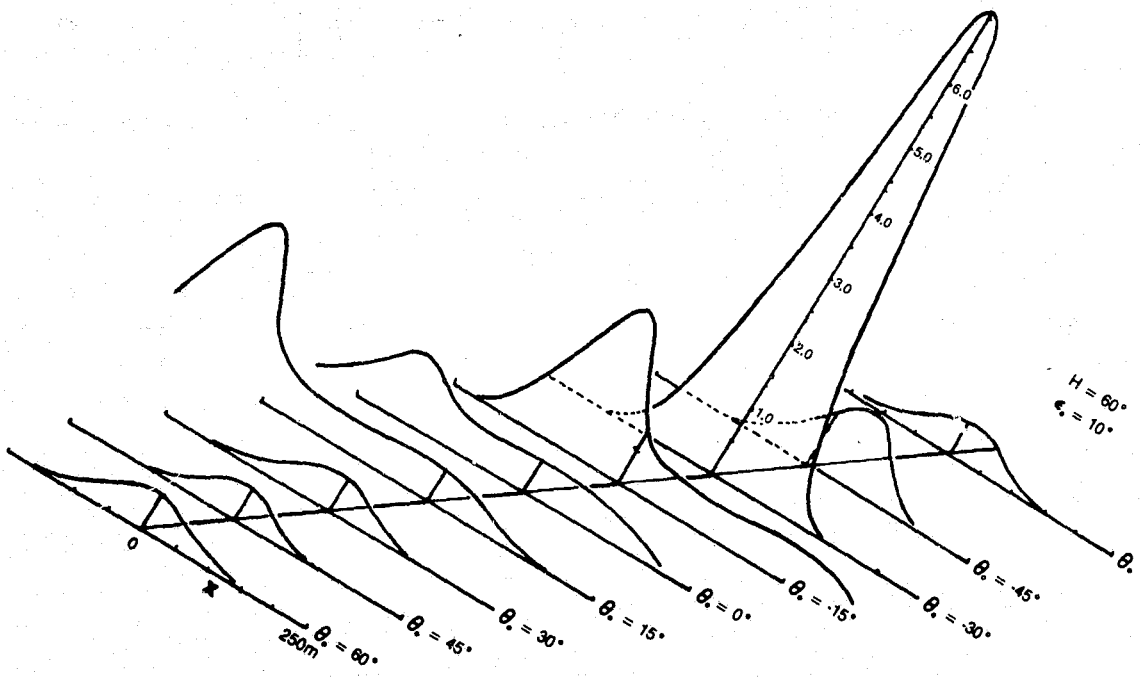

Figure II.5. Graphs showing the radar signal returned by anisotropically scattering targets when they are intercepted by a conically scanning Gaussian beam (3dB width = 1.7°) during horizontal flight past the radar. The targets are assumed to have an air speed equal to the wind speed and to have a common heading (H) relative to the wind direction. The angular variation of cross-section is assumed to be of the form: $\sigma = 2.4 \{2.7 \exp (2.8 \frac{\phi^2}{14}) + 0.2\}$ cm^2 which approximately describes the variation observed in Locusta. (ϕ is the angle between normal to the body axis and the position vector.) Vertical axis shows ratio of signal to that returned by a 1 cm^2 target at r_o, θ_o, ε_o (see Fig. II.4).